8th ECCOMAS Thematic Conference on the Mechanical Response of Composites
COMPOSITES 2021
M. Fagerström & C. Catalanotti (Editors)

APPLICATION OF A RATE DEPENDENT MODEL ON A UNIDIRECTIONAL NON-CRIMP CARBON/EPOXY COMPOSITE

V. Singh[1,2,*], R. Larsson[2], R. Olsson[1], E. Marklund[1]

[1] Polymeric materials and Composites, RISE Research Institutes of Sweden, Mölndal, Sweden
[2] Industrial and Material Science, Chalmers University of Technology, Göteborg, Sweden
[*] vivekendra.singh@ri.se

Keywords: Strain rate, NCF, Continuum damage.

Summary: *This paper presents a novel material model for the simulation of strain rate and damage growth in unidirectional carbon non-crimp fabrics reinforced epoxy (NCF) composite in transverse compression. Therefore, a viscoelastic-viscoplastic model for the matrix and a transversely isotropic model for the carbon fibres together with continuum damage is introduced. The model is based on computational homogenization with a subscale represented by matrix and fibre constituents at finite deformation. The developed material model is implemented in Abaqus/Explicit. A good agreement between the finite element model response and the observed experimental data for transverse compression tests is obtained.*

1. INTRODUCTION

Carbon fibre reinforced polymer composites offer high specific stiffness and strength as well as an adjustable energy absorption capacity [1]. Therefore, they are well suited for developing lightweight structures in aviation, vehicle constructions and machine building. On the other hand, textile technology, offers economically attractive alternatives to the traditional pre-preg composites. The NCF composites have attracted the attention of industries, offering lower manufacturing costs and improved through-thickness properties with no significant drop in the in-plane performance. Due to the complex architecture of NCF materials, they have not yet achieved the necessary level of development for dynamic applications.

The strain rate dependence of composites reinforced by unidirectional fibres or textiles has been investigated in several experimental studies [2, 3, 4]. For dynamic strain rates split Hopkinson bars are frequently used. The results are reviewed by Singh [5] and Sierakowski [6]. Extensive experimental studies of uniweave NCF have also been done by Bru et al. [7] at quasi-static strain rates. Recently, compressive and tensile loading tests at different strain rates were performed on the uniweave NCF composite considered in this paper [9].

There are a few dynamic constitutive models addressing the nonlinear strain rate effect coupled to damage growth and anisotropy but only limited to unidirectional composites. Models by Gerbaud et al. [10] and Eskandaria et al. [11] used phenomenological invariant based formulations to represent viscoelastic/viscoplastic effects in polymer composites but without damage growth. A micromechanics based model for unidirectional polymer composites under

quasi-static and high strain rates was proposed by Larsson et al. [12], where the matrix is assumed to be viscoelastic-viscoplastic while the carbon fibres are elastic transversely isotropic. Recently, this model was extended to include continuum damage in unidirectional composites [13]. In this paper, the model by Larsson et al. [12, 13] is utilized to simulate dynamic behaviour of a uniweave NCF composite, due to the similarities with unidirectional prepregs.

2. Implementation of homogenized matrix-fibre response

This section describes the computational homogenization technique used to relate the sub-scale matrix-fibre response to the macroscale.

Consider a Representative Volume Element (RVE) $B^0_\square$ of the fibre/matrix composite as shown in Figure 1. The matrix material is defined by the region $B^{0,m}_\square$ and the fibre material by the region $B^{0,f}_\square$ in the RVE.

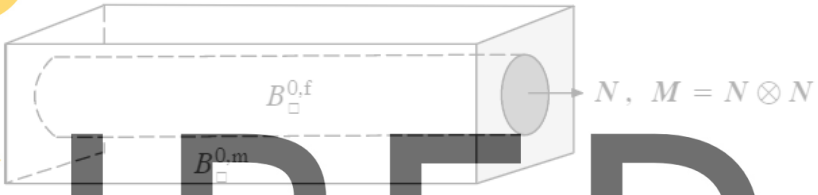

Figure 1: Representative volume element with volume $V_\square$ with a fibre region $B^{0,\mathrm{f}}_\square \in B^0_\square$ (with the fibre orientation M) embedded into the polymer matrix $B^{0,\mathrm{m}}_\square$ in $B^0_\square$.

To describe the microscopic lagrangian strain field $\boldsymbol{E}$ locally in $B^0_\square$, it is assumed that the microscopic strain field $\boldsymbol{E}$ split into a macroscopic, constant (average) strain $\bar{\boldsymbol{E}}$ in the RVE (where $\bar{\boldsymbol{E}}$ is the macroscopic displacement of the solid), and a fluctuating portion $\tilde{\boldsymbol{E}}$.

$$\boldsymbol{E} = \bar{\boldsymbol{E}} + \tilde{\boldsymbol{E}} \in B^0_\square \tag{1}$$

Following [12], a Hill-Mandel condition is used to derive the homogenized response of the deformation process in the RVE. It states that the homogenized virtual work done by the macroscopic strain and stress equals the virtual work done by the microscopic strain and stress fields in the RVE.

$$\delta\bar{\boldsymbol{E}} : \bar{\boldsymbol{S}} = \delta\bar{\boldsymbol{E}} :< (\boldsymbol{I} + a\,\boldsymbol{I}_{\bar{E}}) : \boldsymbol{S} >_{B^0_\square} + \hat{\boldsymbol{E}} :< \delta a\,\boldsymbol{S} >_{B^0_\square} \quad \forall \delta a \tag{2}$$

where, S is the homogenized (continuum) stress in the material form.

A simple but realistic representation of the homogenized response of the composite has been implemented by assuming a constant strain (Voigt model) in the fibre direction, even in the non-linear regime of the micro-mechanical response. A constant stress (Ruess model) is used in the transverse direction of the fibres. The fluctuation is most significant with respect to the transverse direction of the fibre.

To formulate the strain fluctuation a piecewise constant scalar field a in $B^0_\square$ is assumed where $\hat{\boldsymbol{E}}$ is the projected macroscopic strain tensor onto the transverse direction of the fibre.

$$\tilde{\boldsymbol{E}} \coloneqq a\,\hat{\boldsymbol{E}} \tag{3}$$

where

$$a = \begin{cases} a^{\mathrm{f}} & \boldsymbol{X} \in B^{0,\mathrm{f}}_\square \\ a^{\mathrm{m}} & \boldsymbol{X} \in B^{0,\mathrm{m}}_\square \end{cases}, \boldsymbol{S} = \begin{cases} \boldsymbol{S}^{\mathrm{f}} & \boldsymbol{X} \in B^{0,\mathrm{f}}_\square \\ \boldsymbol{S}^{\mathrm{m}} & \boldsymbol{X} \in B^{0,\mathrm{m}}_\square \end{cases} \tag{4}$$

Upon inserting these expressions into the Hill-Mandel condition, (eq 2), we find that the homogenized (continuum) stress in is obtained as

$$\bar{\boldsymbol{S}} = < \left(\boldsymbol{I} + a\,\hat{\boldsymbol{I}}\right) : \boldsymbol{S} >_{B^0_\square} = v^{\mathrm{m}}\,\boldsymbol{S}^{\mathrm{m}} + v^{\mathrm{f}}\,\boldsymbol{S}^{\mathrm{f}} + a^{\mathrm{m}}\,v^{\mathrm{m}}\,\hat{\boldsymbol{I}} : \left(\boldsymbol{S}^{\mathrm{m}} - \boldsymbol{S}^{\mathrm{f}}\right) \tag{5}$$

The homogenization in spatial form follows as

$$\bar{\boldsymbol{\tau}} = < \left(\boldsymbol{I} + a\,\hat{\boldsymbol{i}}\right) : \boldsymbol{\tau} >_{B^0_\square} = v^{\mathrm{m}}\boldsymbol{\tau}^{\mathrm{m}} + v^{\mathrm{f}}\boldsymbol{\tau}^{\mathrm{f}} + a^{\mathrm{m}}v^{\mathrm{m}}\hat{\boldsymbol{i}} : \left(\boldsymbol{\tau}^{\mathrm{m}} - \boldsymbol{\tau}^{\mathrm{f}}\right) \tag{6}$$

together with

$$\left(\boldsymbol{\tau}^{\mathrm{m}} - \boldsymbol{\tau}^{\mathrm{f}}\right) : \hat{\boldsymbol{e}} = 0 \text{ with } \hat{e} = \hat{\boldsymbol{i}} : \bar{e} \text{ and } \bar{e} = \frac{1}{2}\left(1 - \bar{b}^{-1}\right) \tag{7}$$

Here, $\hat{e}$ is the projected Eulerian strain tensor $\bar{e}$ onto the transverse fibre direction. $\boldsymbol{\tau} = \bar{F}\cdot\boldsymbol{S}\cdot\bar{F}^t$ is the Kirchhoff stresses in the spatial form. A more in detailed explanation and discussion of this implementation is given in [13].

2.1 Constitutive response of matrix and fibre constituents

This section describes the model developed for the matrix and the fibre constituents. This development represents [12] and it's extension to include a damage enhanced effective matrix material model [13].

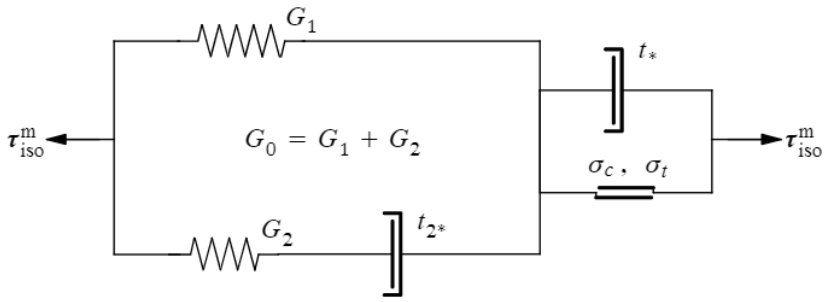

Figure 2: Rheologcial model for viscoelastic-viscoplastic response of the polymer matrix of the composite.

To model the polymer matrix, a rheological model in Figure 2 for the viscoelastic-viscoplastic coupling is considered. This coupling is described by six parameters. A quasi-static and dynamic shear moduli, G_1, G_0 (via G_2) and the visco-elastic damper t_{2*} represent linearly viscoelastic response. This is coupled with the viscoplastic response defined by the σ_t, σ_c defining the quasi-static yield stress of the polymer matrix in tension and compression and the viscoplastic damper t_*.

In order to model the matrix material we consider the stored free energy ψ^{m} related to the volume of matrix material in the RVE. This is defined as

$$\psi^{\mathrm{m}} = f[\alpha]\left(\hat{\psi}^{\mathrm{m}}_{1,iso} + \hat{\psi}^{\mathrm{m}}_{2,iso}\right) + \psi^{\mathrm{m}}_{vol} \tag{8}$$

representing the deviatoric (or shape distortion) energy and the volume change energy of the matrix material.

Using the basic postulate of the mechanical dissipation rate $\mathcal{D}^{\mathrm{m}} \geq 0$ we obtain the total Kirchhoff stress of the matrix as

$$\boldsymbol{\tau}^{\mathrm{m}} = f[\alpha]\hat{\boldsymbol{\tau}}^{\mathrm{m}}_{iso} + \tau^{\mathrm{m}}_m \mathbf{1} \text{ with } \hat{\boldsymbol{\tau}}^{\mathrm{m}}_{iso} = \hat{\boldsymbol{\tau}}^{\mathrm{m}}_{1,iso} + \hat{\boldsymbol{\tau}}^{\mathrm{m}}_{2,iso} \tag{9}$$

$f[\alpha]$ is the damage degradation function degrades only the matrix

$$f[\alpha] = (1-\alpha)^2 + r \tag{10}$$

whereby $f'[\alpha] < 0$ for $0 \leq \alpha \leq 1$.

We introduce the viscoplastic-viscoelastic evolution rules related to the matrix shear behaviour defined as

$$\boldsymbol{d}_p = \lambda \frac{\partial \phi^*}{\partial \hat{\boldsymbol{\tau}}^{\mathrm{m}}_{iso}} = \lambda \boldsymbol{f} \text{ with } \boldsymbol{f} = \frac{3}{2}\frac{\hat{\boldsymbol{\tau}}^{\mathrm{m}}_{iso}}{\hat{\tau}^{\mathrm{m}}_e} \tag{11a}$$

$$\boldsymbol{d}_v = \frac{1}{2G_2 t_{2*}} \hat{\boldsymbol{\tau}}^{\mathrm{m}}_{2,iso} \tag{11b}$$

λ is the viscoplastic multiplier obeys the Bingham model

$$\lambda = \frac{1}{t_*}\eta[\phi] \geq 0 \text{ with } \eta[\phi] := \frac{< \hat{\tau}^{\mathrm{m}}_e - (c_y + \gamma p) >}{3G_0} \tag{12}$$

where t_* is the viscoplastic relaxation time and η is the Bingham overstress function.

For the carbon fibres, a transversely isotropic hyper-elastic response is assumed. The total elastic response is obtained from the stored free energy ψ^{f} defined as

$$\psi^{\mathrm{f}} = \psi^{\mathrm{f}}_d + \psi^{\mathrm{f}}_{vol} + \psi^{\mathrm{f}}_s + \psi^{\mathrm{f}}_a \tag{13}$$

Hyperelastic response of fibre material in terms of the 2nd Piola Kirchhoff stress is

$$\boldsymbol{S} = \frac{\partial \psi^{\mathrm{f}}}{\partial \boldsymbol{E}} = \boldsymbol{S}^{\mathrm{f}}_d + S^{\mathrm{f}}_m \mathbf{1} + \boldsymbol{S}^{\mathrm{f}}_s + S^{\mathrm{f}}_a \boldsymbol{M} \tag{14}$$

Push forward to spatial coordinates yields the Kirchhoff stress as $\boldsymbol{\tau}^{\mathrm{f}} = \bar{\boldsymbol{F}} \cdot \boldsymbol{S}^{\mathrm{f}} \cdot \bar{\boldsymbol{F}}^t$. This gives the total Kirchhoff stress as $\boldsymbol{\tau}^{\mathrm{f}} = \boldsymbol{\tau}^{\mathrm{f}}_d + \boldsymbol{\tau}^{\mathrm{f}}_m + \boldsymbol{\tau}^{\mathrm{f}}_s + \boldsymbol{\tau}^{\mathrm{f}}_a$.

3. Continuum damage, Material data and Numerical examples

In this section, continuum damage evolution, material data and the numerical examples are discussed. To predict the onset and evolution of global failure of the composite a damage model is exploited. Following the developments in [13, 14], damage evolution $\dot{\alpha}$ is coupled to the viscoplastic part of the matrix model, where the damage variable α degrades the matrix material as in eq.(9). In this paper rate dependent local damage model is advocated, involving the fracture energy $\mathcal{G}_c$, the internal length parameter l_c and the damage progression speed parameter v^*. The model is applied on a chosen geometry and material in order to demonstrate the capabilities of the proposed model for simulating the dynamic behaviour of an NCF composite.

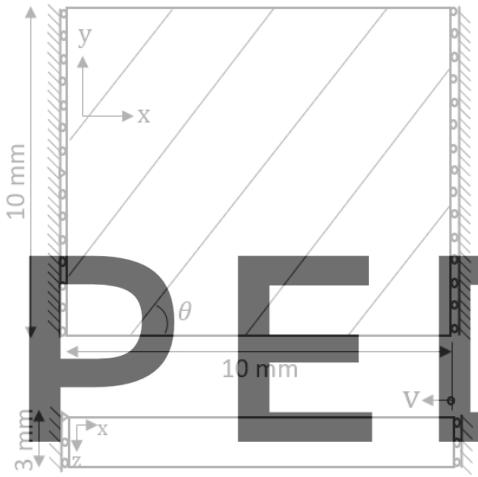

Figure 3: Specimen geometry for HTS45-LY556 NCF composite laminates subjected to transverse compression loading through the prescribed horizontal velocity v at the right edge.

The rate dependent damage model developed in [13] is implemented in the finite element (FE) code Abaqus/Explicit to simulate transverse compression tests through the user defined material subroutine VUMAT. The 8-node reduced integration, C3D8R solid element with dimensions of $0.1 \times 0.1 \times 0.1$ mm^3 is used to discretize the ply. The backward Euler method is used to integrate the viscoelastic-viscoplastic flow rules and a radial return mapping algorithm implemented to update Cauchy stress.

Table 1: Considered applied loading rates and consequent (homogeneous) compressive strain rates for the fibre off-axis specimens [7, 9].

	Strain rates in compression [/s]		Loading rate v [mm/s]		Estimated
Fibre angle θ	Quasi-static	Dynamic	Quasi-static	Dynamic	v^* [mm/s]
90°	2.5×10^{-3}	496	0.025	4960	5000
90°	-	984	-	9840	10000

Table 2: Material parameters for the carbon fibre.

E_L^{f}	E_T^{f}	G_{LT}^{f}	G_{TT}^{f}	K_{vol}^{f}	ν_{LT}^{f}	ν_{TT}^{f}	v^{f}
GPa	GPa	GPa	GPa	GPa	-	-	%
240	24	30	9.0	24.6	0.25	0.5	60

Table 3: Material parameters for the epoxy at quasi-static loading.

E^{m}	ν^{m}	$G_1 = G^{\mathrm{m}}$	K^{m}	σ_t	σ_c	$\mathcal{G}_{\mathrm{c}}$
GPa	-	GPa	GPa	MPa	MPa	N/mm
4.9$^{\bullet}$	0.35	1.81	5.44	73	106	0.09

The material consists of epoxy reinforced by a unidirectional non-crimp fabric (NCF). The NCF is a Porcher 4510 "uniweave" with 96.5 percent HTS45 carbon fibres and 3.5 percent glass/polyamide weft yarns. The epoxy consists of Araldite LY556 epoxy resin, an Aradur HY917 hardener and a DY070 accelerator with weight proportions 100/90/0.5 ("System 1") [16]. The test specimen, subjected to uniaxial compression under quasi-static and dynamic loading, is shown in Figure 3. The quasi-static experiment on the NCF composite was performed by Bru et al. [7] in tension and compression. Recently, Olsson et al. [9] performed dynamic tests on off-axis specimens of the same material system in tension and compression.

The elastic fibre properties are shown in Table 2. The longitudinal modulus is according to the manufacturers data [15] and other fibre properties are estimated. The adopted properties for LY556 epoxy (shown in Table 3) are obtained from [16], except [17] for compressive strength and in-house data for tensile strength. To improve the stiffness prediction of the model for shear and transverse loading of the composite in the viscoelastic range the elastic modulus of the resin was corrected by an enhancement factor 1.53. The factor was selected to obtain a good match with the Halpin-Tsai expressions, which account for the inhomogeneous stress state in fibre composites. This correction is indicated by • marker.

3.1 Calibration and model parameters

This section summarizes the steps for the determination of model parameters associated with the material system, HTS45/LY556.

The model parameters are shown in Table 4. The procedure for determining the viscoelastic and viscoplastic model parameters has been thoroughly explained in [12, 13]; a brief summary is given here.

Some of the model parameters are estimated. The damage parameter l_c is estimated based on the order of the distance between the fibres in UD composites, i.e. ca.0.005 mm. Furthermore, v^* should be higher than the applied loading rate i.e. $v^* > v$ to properly capture the damage localization in FE simulation. For others, a calibration method is used to find the best

Table 4: Model parameters for neat epoxy matrix material. The damage progression velocity parameter v^* is adjusted for each test case (see Table 1) as indicated by the ★ marker.

Calibrated			Estimated	
G_2	t_{2*}	t_*	l_c	v^*
GPa	s	s	mm	mm/s
250	1.12×10^{-6}	9.50	0.005	★

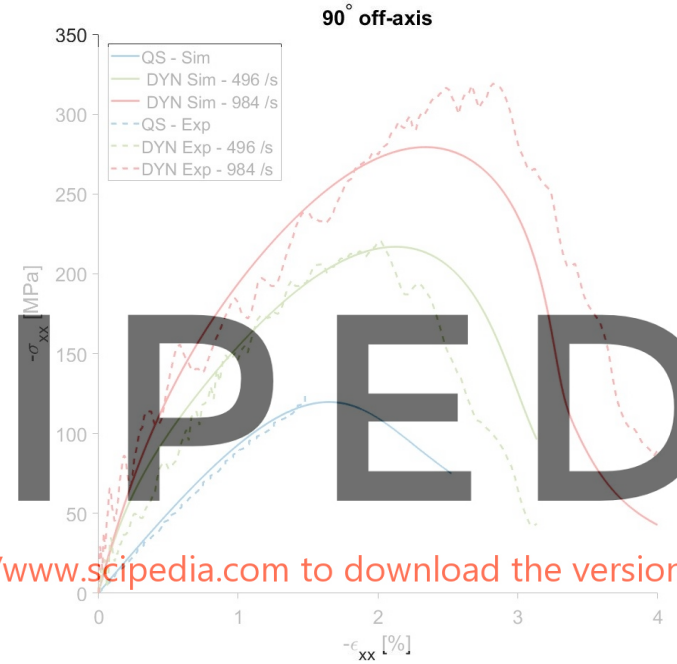

Figure 4: Comparison of experiment and material point stress-strain predictions under uniaxial transverse compression after calibration to the material parameters listed in Table 2 and 3.

possible value using the least square fit. Like in [12, 13], the calibration is carried out, using a MATLAB/FORTRAN implementation, for uniaxial compression tests at the material point level. Both quasi-static and dynamic tests are included in the calibration.

The calibrated model parameters for the 90° off-axis case are shown in Table 4. Figure 4 shows the good correlation between experiment and the calibrated response.

3.2 Validation

This section describes the validation of the material model at rate dependent intralaminar failure predictions of the NCF composite in transverse compression. The FE model predictions are compared with the experimental response of the NCF composite specimen at different strain

rates.

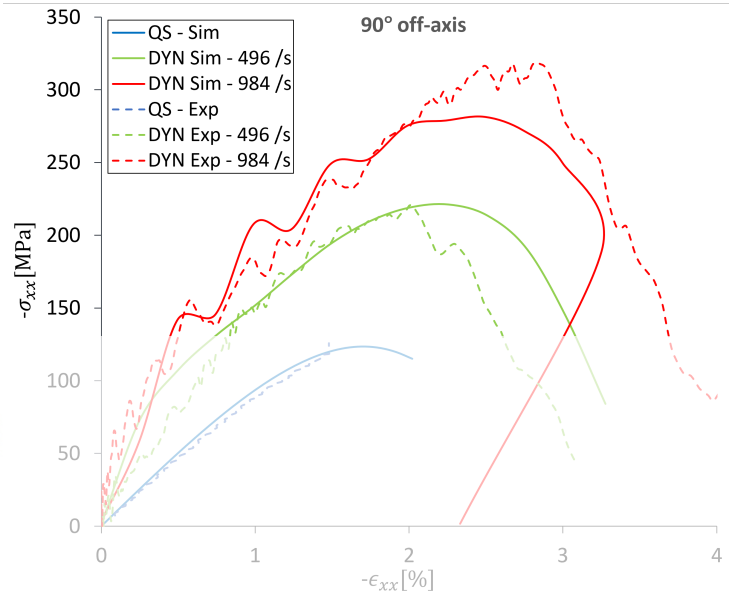

Figure 5: Comparison of experiment and FE stress-strain predictions of the complete specimen in Figure 3 under uniaxial transverse compression at different strain rates.

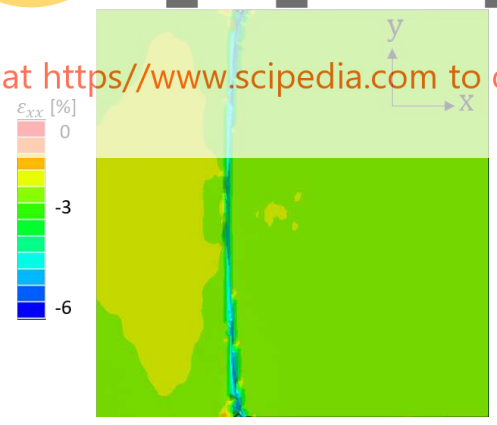

(a) In-plane strain ϵ_x at 496 /s

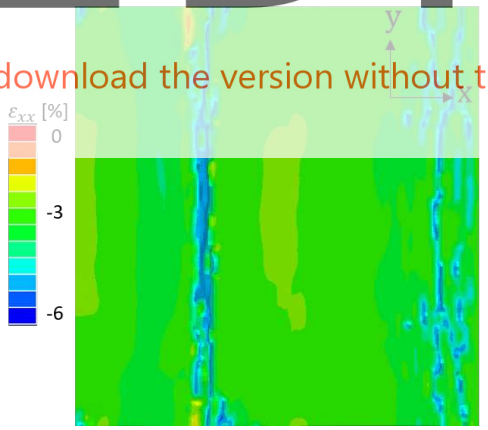

(b) In-plane strain ϵ_x at 984 /s

(c) Out-of-plane crack growth at 496 /s

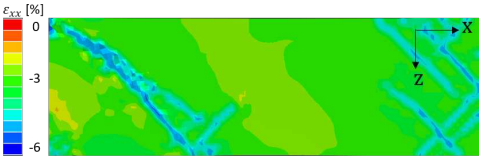

(d) Out-of-plane crack growth at 984 /s

Figure 6: FE predictions for dynamic failure of 90° off-axis specimen in compression.

There is a good qualitative agreement between experiment and simulation results in Figure 5. The FE-based stress strain response agrees well for the quasi-static and dynamic loading of 984 /s, whereas initially a too stiff response is obtained for the dynamic loading of 496 /s while later FE-predictions agree well.

Figure 6 shows axial strain distribution ϵ_x from the FE predictions of the dynamic compressive failure in the NCF. A localized transverse in-plane behaviour is observed for both strain rates, cf. Figures 7a-7b, whereas 45° out-of-plane shear bands are observed in the x-z plane, cf. Figures 7c-7d. At 496 /s, a single out-of-plane shear band is observed, whereas multiple out-of-plane shear bands are observed at 984 /s in the x-z plane. The damage patterns agree well with the dynamic transverse compression test performed on IM7/8552 material system by Koerber et al. [2].

4. Conclusions

A recent rate dependent micromechanically based model [12], extended by continuum damage, has been presented to predict the out-of-plane intralaminar failure modes of an NCF composite in transverse compression. The model predictions are in good agreement with the considered transverse compressive experimental results of the NCF composite at both quasi-static and dynamic strain rates. The increase in stiffness and strength together with softening due to the progressive damage at increasing strain rates is successfully captured by the model. The different failure modes of the composite under transverse compression are in line with other relevant studies [2].

5. Acknowledgement

The financial support for this work has been provided by the Swedish Foundation for Strategic Research (SSF) for funding modelling (dnr FID16-0041). ICONIC project under the Marie Skłodowska-Curie grant agreement No 721256 for funding experiments and RISE internal development funds (SK project - P108811) for co-funding modelling. A particular acknowledgement is due to G. Lampeas and B. Ravindran at University of Patras for experimental data, which allowed us to validate our model.

References

[1] J.J. Carruthers, A.P. Kettle, A.M. Robinson, Energy absorption capability and crashworthiness of composite material structures. *Applied Mechanics Reviews*, **51** 635-649, 1998.

[2] H. Koerber, J. Xavier, P. Camanho, High strain rate characterisation of unidirectional carbon-epoxy IM7/8552 in transverse compression and in-plane shear using digital image correlation. *Mechanics of Materials*, **42** 1004–1019, 2010.

[3] H. M. Hsiao, I. M. Daniel, R. D. Cordes, Strain rate effects on the transverse compressive behavior of unidirectional composites, *J. Compos. Mater.*, **33** No. 17, 1620-1642, 1999.

[4] J. Harding, Effect of strain rate and specimen geometry on the compressive strength of woven glass-reinforced epoxy laminates, *Composites*, **24**, No. 4, 323-332 1993.

[5] V. Singh, Literature survey of strain rate effects on composites. TR18-001 (open), Swerea (now RISE) SICOMP, Mölndal, Sweden, 2018.

[6] R.L. Sierakowski, Strain rate effects in composites, *Applied Mechanics Reviews*, **50**, 741–761, 1997.

[7] T. Bru, P. Hellström, R. Gutkin, D. Ramantani, G. Peterson, Characterisation of the mechanical and fracture properties of a uni-weave carbon fibre/epoxy non-crimp fabric composite, *Data in Brief*, **6**, 680–695, 2016.

[8] B. Song, W. Chen, T. Weerasooriya, Quasi-Static and Dynamic Compressive Behaviors of a S-2 Glass/SC15 Composite, *Journal of Composite Materials*, **37**, 1723–1743, 2003.

[9] R. Olsson, G. Lampeas, B. Ravindran, F. Izerhab, Dynamic testing of a unidirectional NCF composite - a comparison of test methods, *presentation at 10th International Conference on Composites Testing and Model Identification*, Lille, 2021.

[10] P.W. Gerbaud, F. Otero, P. Bussetta, P. Camanho, An invariant based transversely-isotropic constitutive model for unidirectional fibre reinforced composites considering the matrix viscous effects, *Mechanics of Materials*, 138, 2019.

[11] S. Eskandaria, F. Pires, P. Camanho, H. Cuic, N. Petrinica, A. Marques, Analyzing the failure and damage of frp composite laminates under high strain rates considering viscoplasticity, *Engineering Failure Analysis*, **101**, 257–273, 2019.

[12] R. Larsson, V. Singh, R. Olsson, E. Marklund, A micromechanically based model for strainrate effects in unidirectional composites, *Mechanics of Materials*, **148**, 193–212, 2020.

[13] V. Singh, Strain rate dependent material model for polymer composites, *Paper B - Licentiate thesis*, Chalmers University of Technology, 2021.

[14] R. Larsson, R. Gutkin and R. Rouhi, Damage growth and strain localization in compressive loaded fiber reinforced composites, *Mechanics of Materials*, **127**, 77–90, 2018.

[15] Teijin Limited. HTS45 Tenax™ filament yarn product data sheet. URL:https://www.teijincarbon.com/products/tenaxr-carbon-fiber/tenaxr-filament-yarn?r=1.

[16] Huntsman Corporation. Araldite LY556 Aradur 917 Accelerator DY070 (data sheet 03/07/2007). URL:https://farix.hu/pdf/1360669728.pdf.

[17] S. Singh, V.K. Srivastava, R. Prakash, Influences of carbon nanofillers on mechanical performance of epoxy resin polymer, *Applied Nanoscience*, **5**, 305–313, 215.